Label-free Single-molecule Immunoassay

Xiaoyan Zhou[1,2,#], Chao Chen[1,3,#], Guangzhong Ma[1], Mohammad Javad H. N. Chemerkouh[1,2], Christine LH Snozek[5], Eric H. Yang[6], Brandyn Braswell[1,4], Zijian Wan[1,2], Shaopeng Wang[1,3]*

[1]Center for Biosensors and Bioelectronics, The Biodesign Institute, Arizona State University, Tempe, Arizona 85287, United State
[2]School of Electrical, Computer and Energy Engineering, Arizona State University, Tempe, Arizona 85287, United State
[3]School of Biological and Health Systems Engineering, Arizona State University, Tempe, Arizona 85287, USA.
[4]School of Engineering for Matter, Transport and Energy, Arizona State University, Tempe, Arizona 85287, United State
[5]Department of Laboratory Medicine and Pathology, Mayo Clinic Arizona, Phoenix, Arizona 85054, United State
[6]Department of Cardiovascular Disease, Mayo Clinic Arizona, Phoenix, Arizona 85054, United State

[#]These authors contributed equally to this work.

*Corresponding author email: Shaopeng.Wang@asu.edu

Abstract

Single-molecule immunoassay is a reliable technique for the detection and quantification of low-abundance blood biomarkers, which are essential for early disease diagnosis and biomedical research. However, current single-molecule methods all require signal amplification via labelling, which brings a variety of unwanted consequences, such as matrix effects and autofluorescence interference. Here, we introduce a real-time mass imaging-based label-free single-molecule immunoassay (LFSM-immunoassay). Featuring plasmonic scattering microscopy-based real-time mass imaging, a 2-step sandwich assay format-enabled background reduction, and minimization of matrix effects by dynamic tracking of single binding events, the LFSM-immunoassay enables ultra-sensitive and direct protein detection at the single-molecule level in neat blood sample matrices. We demonstrated that the LFSM-immunoassay can measure sub-femtomolar levels of interleukin-6 and prostate-specific antigen in whole blood with 8 log dynamic range. To show its translational potential to clinical settings, we measured NT-proBNP (N-terminal pro-brain natriuretic peptide) in 28 patient serum samples using a 20 minute LFSM-immunoassay, and the results show a strong linear correlation ($r > 0.99$) with clinical lab reported values.

Keywords:

single-molecule, digital immunoassay, label-free, plasmonic scattering microscopy, whole blood, serum, IL-6, NT-proBNP, PSA

Introduction

Detection and quantification of biomarkers at extremely low levels is important to disease detection, monitoring and treatment[1-3]. Although thousands of approaches have been developed, the enzyme-linked immunosorbent assay and its variations remains the commonly-used methods for the detection of protein biomarkers in both clinical use and basic research[4,5]. However, its dynamic range (log 3), detection limit (picomolar range) and assay time (3-8h) fall short of the requirement of early disease diagnosis in clinical settings[6]. Recently, the development of single-molecule imaging has made it possible to visualize individual binding complexes, leading to greatly improved sensitivity, reliability and more depth of information compared to conventional methods[7]. Newer methods – including single-molecule enzyme-linked immunosorbent assays (SiMoAs)[8], single-molecule recognition through equilibrium Poisson sampling (SiMREPS)[9], single-molecule augmented capture (SMAC)[10] and time-resolved digital immunoassay (TD-immunoassay)[11] – have been developed to improve detection limits. However, all of these need to amplify the original binding signal, by means of an enzyme amplification, fluorescence probe or gold nanoparticle probe. Methods based on enzyme amplification and gold nanoparticle labelling are limited by matrix effects and unwanted background signal arising from nonspecific reagent binding to the assay substrate. Fluorescence-based methods are limited by photobleaching and ubiquitous autofluorescence of sample matrix components. Such limitations make these single-molecule assays incapable of measuring biomarkers directly in undiluted complex sample matrices, especially in whole blood.

Here, we introduce a real-time mass imaging-based label-free single-molecule immunoassay (LFSM-immunoassay) which enables ultra-sensitive and direct protein detection in neat blood sample matrices. The LFSM-immunoassay relies on plasmonic scattering microscopy (PSM)[12] to detect individual biomarker immunocomplexes forming on the sensor surface. PSM detects scattered light from single molecules and determines single molecular mass with high spatial and temporal resolution. A 2-step sandwich assay format is adopted in the LFSM-immunoassay so as to separate sample incubation from detection antibody binding. In this way, the sample matrix is washed away, thereby dramatically reducing background signal. As such, PSM can specifically extract and track the binding of single detection antibodies in pure buffer to the biomarker molecules captured on the sensor surface. In addition, LFSM-immunoassay could be less affected by some matrix effects like interfering molecules with structure similar to the biomarker of interest or heterophilic antibodies, which could be ruled out by dynamically tracking the binding events and using binding kinetics-based information to differentiate the nonspecific and specific binding. Last but not least, the label-free nature of the LFSM-immunoassay completely eliminates the influence of labelling reagents, which could not only compromise the binding capability but also cause nonspecific binding. To the best of our knowledge, the LFSM-immunoassay is also the first technology to realize label-free detection of protein biomarkers at single-molecule level. To validate this novel method, we have demonstrated interleukin-6 (IL-6) detection in both buffer and serum. We also evaluated the clinical application of LFSM-immunoassay with N-terminal prohormone of brain natriuretic peptide (NT-proBNP), an important biomarker for heart failure, and demonstrated excellent linear correlation with commercial Elecsys proBNP II assay. Finally, our method is also the first to realize sub-femtomolar biomarker detection in undiluted whole blood samples. Therefore, we believe that the LFSM-immunoassay is a promising novel method that could revolutionize in-vitro diagnostics.

Results

Principle and Setup

In LFSM-immunoassay, individual biomarkers of interest were pulled down by a capture antibody which was pre-immobilized on a gold-coated glass slide via a polyethylene glycol (PEG) linker (Figure 1a). The surface density of capture antibody was controlled by adjusting the molar ratio between the PEG linker and spacer molecules to avoid steric hindrance effect (Figure 2a). Detection antibodies were then introduced to bind with the biomarkers caught by the antibody, and the binding process was read out by PSM[12]. The optical layout of the prism-coupled PSM setup is shown in Figure S1, which is a simplified version from our previous design[13]. Briefly, a p-polarized light from a red laser was directed on the gold surface to excite surface plasmon resonance (SPR) and the associated evanescent field via a prism. The scattered light within the field was collected by an objective placed on top of the microchip and imaged with a COMS camera, which recorded the dynamic binding process of single detection antibodies with a temporal resolution of ~ 10 ms (Figure 1a, Figure 1b). Single binding events were tracked using an optimized data analysis approach, which provided high quality images and precise information of the single molecular binding events in the illuminated sensor surface. Based on the position, duration, and intensity of each individual binding event, the number of detection antibodies specifically binding to the captured biomarker was counted over time, and the standard curve for measuring the biomarker concentration was obtained (Figure 1b).

Ultra-sensitive quantitation was achieved by the optimized data analysis approach (Figure S11). Frist, the noise in the image was reduced by a n frame rolling averaging in the raw video starting at frame m, N_m^{m+n}, and then the intensity of each frame of the averaged video was normalized by their mean pixel intensity value to avoid the influence of light source intensity fluctuation (see support information for more details). Next, a differential image sequence ($N_{m+n}^{m+2n} - N_m^{m+n}$) was obtained from the normalized image sequence by subtracting each frame from the following frame, which removed static background and revealed binding or unbinding events. Second, a probability image (PI) sequence was obtained by convoluting the differential image sequence with Haar-like array, which would reveal the morphological characteristics of the particle[14]. The candidate pixels were selected if their intensity was higher than the mean intensity + 3 × standard deviation (s.d.) of the whole PI. Third, a fixed region was extracted in the differential images at positions of the candidate pixels mapped from the PI and fitted with a 2D Gaussian model to obtain the precise center location and intensity of the particle[15]. The candidate pixels with a fitting biased too much from a Gaussian blob would be deleted[16]. Last, as the binding of a particle appears as a brightening Gaussian blob and then gradually disappears (Figure S12), the intensity of the single particle was determined as the peak of its temporal intensity profile. Additional details of data analysis are provided in Supplementary Notes 1 and 2.

Because of the interference with surface roughness scattered light, a linear relationship between PSM image intensity of molecules and their molecular weight (MW) has been established[12,17]. Such linear intensity-mass relationship was confirmed on our PSM setup with four different sized pure protein samples (Figure 2b). With this information, whether a bound single particle was detection antibody was determined based on its intensity. The binding events were also considered nonspecific if they happened at the same location multiple times, based on probability

consideration (Supplementary Note 2). The difference between specific and nonspecific binding is shown in the supporting video. These analyses are critical for removing confounding effects caused by complex sample matrices like blood and greatly improved the counting accuracy.

Validation of label-free assay by IL-6 detection

To assess the intrinsic sensitivity of LFSM-immunoassay, we first applied it to detection of IL-6, a key factor in hematopoiesis, immunomodulation and inflammation processes[18-20], in pure buffer (1x PBS containing 1% BSA) and bovine serum. A series of standard buffer solutions or spiked bovine serum samples with different concentrations of IL-6 were flowed through the microfluidic channel for 2 hours to react with the capture antibody pre-functionalized on the sensor surface. Next, 10 nM detection antibody was injected for 10 min to bind with IL-6 captured by the surface antibody, which is monitored by PSM (Figure 2a). The number of IL-6 caught on the sensor surface was tracked by counting the binding events of the detection antibody with a temporal resolution of ~10 ms. The temporal profile of the binding events follows the association kinetics of binding and correlates with the concentration of IL-6 (Figure 2c and 2d).

The standard curves for IL-6 detection in pure buffer and bovine serum were determined in triplicates for each concentration (Figure 2e). Defined as the mean counts of blank experiments plus three times the standard deviation (s.d.), the limits of detection (LOD) are calculated to be 6.18 fg/mL and 4.91 fg/mL (0.29 fM and 0.23 fM) in pure buffer and bovine serum, respectively. The level of nonspecific binding events in bovine serum was lower than in pure buffer, as bovine serum could block the sensor surface better. For clarity, only part of the data are shown in Figure 2c - 2e; complete data can be found in the supporting information (Figure S4 and S5). We have realized an 8 log detectable dynamic range, from 6.18 fg/mL to 0.21 μg/mL (Figure S3). The sub-femtomolar sensitivity and wide dynamic range of the label-free assay resulted from two unique factors of real time single molecule imaging: (i) most of the nonspecific bindings were removed based on the intensity, duration and morphology of the binding events, and (ii) dynamic tracking of single particle binding is less limited by the spatial optical resolution and capable of detecting binding signal even when the surface is crowded by particles.

Rapid NT-proBNP detection under clinical setting

Simple, rapid and sensitive assays are always needed in clinical setting[21,22]. To show the applicability of LFSM-immunoassay for clinical use, we evaluated its performance on the rapid detection of NT-proBNP, a key clinical biomarker of heart failure[23-25]. As NT-proBNP is naturally present in human blood, we first measured the baseline level of NT-proBNP in the human plasma pool used for spiking, which was determined to be 8.23 pg/mL (Figure S17). A series of standard samples with different concentrations of NT-proBNP were prepared by spiking recombinant NT-proBNP into the human plasma pool with baseline level correction. To evaluate the background level, horse serum was used as a blank control without human NT-proBNP. For rapid detection, these standard samples were introduced into the microfluidic channel for only 10 min (Figure 2a). Then, 50 nM detection antibody was injected for 10 min. 50 nM was selected for sufficient count with in the detection time frame while keeping a low nonspecific binding level (Figure S16). The same PSM setup and parameters as IL-6 detection were used. The temporal profiles of the binding events are shown in Figure 3a. After repeating the experiments 3 times, the standard curve for NT-

proBNP detection in human plasma was established (Figure 3b). The LOD was determined to be 4.70 pg/mL.

To evaluate the translational potential of LFSM-immunoassay, a cross-validation between the Roche Elecsys proBNP II assay, an FDA-cleared routine clinical diagnostic test for heart failure, was conducted. Serum samples from 28 patients were measured using both the Elecsys proBNP II assay and LFSM-immunoassay. The results were linearly correlated between the two methods (Figure 3c, s1ope = 1.01 and R > 0.99). All measured NT-proBNP concentrations are listed in the table shown in Figure 3d. Overall, we have realized sub-picomolar detection of NT-proBNP with a 20-min total assay time. The dynamic range and detection limit of LFSM-immunoassay also satisfies the requirement for clinical NT-proBNP testing. Therefore, these results indicates that LFSM-immunoassay has a high potential for clinical application.

Protein detection in whole blood

As modern medicine greatly depends on clinical testing for disease diagnosis and patient monitoring, a simple assay for direct analysis of whole blood components is always preferred[26,27]. Detection methods using whole blood as the sample matrix could not only reduce the loss of biomarkers caused by physiolysis and manual operation, but also minimize total assay time by eliminating sample preparation steps, thus making the method compatible with point of care (POC) settings. Recent single-molecule technologies, like single molecule enzyme-linked immunosorbent assay and single molecule fluorescence microscopy[7,8], either require removal of blood cells or have to dilute whole blood to achieve reliable detection due to matrix effects or extreme background autofluorescence. We realized LFSM-immunoassay detection of protein biomarkers at the single molecule level in undiluted whole blood, because it has the following three innovative features: 1) The use of microfluidic flow for the analyte capture step helps to reduce the surface blocking effect caused by red blood cells. 2) The label-free nature, together with the two-step assay format, dramatically lowers the background signal by separating signal readout from biomarker surface capture in whole blood, enabling reliable detection of single binding events. 3) Real-time PSM imaging removes unspecific background signals and reduces matrix effects.

To validate the capability of LFSM-immunoassay for whole blood detection, we measured IL-6 and prostate-specific antigen (PSA)[28-31] directly in whole blood. Bovine whole blood was spiked with different concentrations of IL-6 and PSA. These spiked whole blood samples were measured using LFSM-immunoassay following the same procedure as in IL-6 detection. The temporal profiles of binding events were plotted in Figure 4a and 4c respectively. The standard curves of PSA and IL-6 detection in whole blood were determined after repeating the experiments 3 times (Figure 4b and 4d). The LOD of whole blood PSA was 23.30 fg/mL (0.73 fM) and that for IL-6 was 13.60 fg/mL (0.65 fM). As expected, the slopes of the two standard curves were different due to the difference in affinity of the two antibody pairs. These results demonstrate that LFSM-immunoassay is able to quantify protein biomarker concentrations in undiluted whole blood.

Discussion

Overall, the feasibility and performance of LFSM-immunoassay were demonstrated with our data. To the best of our knowledge, this work is the first to realize ultra-sensitive and rapid digital protein detection with label-free single-molecule technology. Our method shows performance comparable to other single-molecule assays and possesses the ability to detect individual biomarkers in undiluted complex clinical fluids, such as serum, plasma, and whole blood, which has not been previously reported using single-molecule technologies. This also demonstrates that LFSM-immunoassay has reduced matrix effects and removed the nonspecific background noise, which are the limitations of other single-molecule technologies.

The focus of this work is to introduce a new single-molecule technology with acceptable analytical performance that can overcome the limitations of signal amplification to facilitate POC compatibility. LFSM-immunoassay reports the total binding events N(T) of detection antibody on the surface as output signal, which is defined as

$$N(T) = \int_0^T k_{on}[A]_t[P]_t dt$$

where k_{on} is the association rate constant of the detection antibody, $[A]_t$ and $[P]_t$ are the concentrations of available surface bound analyte and detection antibody at time t. Therefore, the signal of LFSM-immunoassay would still increase even after detection antibody binding reaches dynamic equilibrium, which makes it superior to conventional endpoint assays for detecting low-abundance biomarkers[32].

It is worth noting that the accuracy and sensitivity of LFSM-immunoassay are primarily limited by the number of the binding events enumerated, which could be improved by increasing field of view (FOV) or reaction time. We compared the results for the detection antibody reaction time of 5 min or 10 min and it shows that longer reaction time improve the accuracy and sensitivity (Figure S18). However, clinically acceptable assay times and the effects of antibody dissociation restrict the maximum length of reaction time. Increasing FOV may also affect the performance of LFSM-immunoassay by lowering camera frame rate and temporal resolution, such that less information could be collected in the binding duration. A more powerful light source is also needed to enable single-molecule sensitivity in larger FOV and the resultant heating effect would affect the performance of the assay as well[33]. Fortunately, imaging technologies powered by machine learning could possibly enable the detection of IgG antibody at lower exposure time, allowing larger FOV imaging with higher frame rates[34].

LFSM-immunoassay still suffers from some limitations. In the current set-up, LFSM-immunoassay uses an incident illumination intensity of ~ 2 kW/cm^2 to image single detection antibodies with acceptable signal-to-noise ratio (SNR). Higher SNR could improve the accuracy of dynamic counting of single binding events by increasing the incident light intensity. However, the protein molecules on the surface could be damaged due to photothermal effects[13]. Switching the detection technology from PSM to Evanescent Scattering Microscopy (ESM)[35], which uses glass substrate without gold coating, can reduce the photothermal effect.

As a sandwich assay, the affinity of antibodies would influence the performance of LFSM-immunoassay. Most commercial antibodies with nanomolar K_D are compatible with LFSM-immunoassay[36]. However, detection antibodies with k_{on} lower than $10^4\ M^{-1}s^{-1}$ would result in insufficient number of binding events detected in the assay time. A possible solution to improve these slower antibody binding kinetics is to conjugate two low-affinity antibodies together through DNA-based super-assembly technology[37].

Despite these limitations, LFSM-immunoassay shows obvious advantages compared with other digital immunoassays, such as SiMoAs, SiMREPS and SMAC. The label-free nature of LFSM-immunoassay avoids the cost associated with fluorescence probes. By adding an air objective on the top of the imaging area, LFSM-immunoassay could be implemented on commercial SPR systems, which would promote the translation of LFSM-immunoassay into clinical practice. The ability to detect individual biomarkers in undiluted complex clinical fluids could greatly simplify the workflow of clinical testing. Compared with label-free methods like interferometric scattering mass spectrometry (iSCAMS) and surface plasmon resonance (SPR)[38-40], LFSM-immunoassay excels at distinguishing between specific binding of detection antibody to analyte and nonspecifically absorbed biomolecules from the complex media. Therefore, LFSM-immunoassay is a novel digital immunoassay technology for high performance in vitro diagnostics and fundamental biological research with the potential of moving digital immunoassay into clinical applications.

Conclusion

In this work, we have developed a label-free digital kinetic immunoassay that can overcome the limitations of single-molecule immunoassays to enable specific, rapid, and ultrasensitive detection of molecular biomarkers in highly complex sample matrices, including undiluted serum, plasma and whole blood. We validated LFSM-immunoassay using an IL-6 antibody pair that is well-characterized and commercially available, and realized sub-femtomolar detection in pure buffer, undiluted serum, and whole blood. A dynamic range of 8 logs was achieved, which is better than most existing technologies. The results of IL-6 detection in different sample matrices indicates that the interfering substances in biological samples influence the LOD and sensitivity of the assays. LFSM-immunoassay for rapid detection of NT-proBNP in plasma shows better sensitivity, wider dynamic range, and much shorter sample-to-result time than ELISA. When applied to serum samples from patients with heart failure, LFSM-immunoassay exhibits excellent correlation with a FDA-cleared routine clinical diagnostic test, showing its strong potential for clinical translation. Furthermore, ultra-sensitive detection of important clinical biomarkers (IL-6 and PSA) in undiluted whole blood showcases the possibility of moving the LFSM-immunoassay towards POC testing as it completely eliminates sample preparation and the relevant loss of biomarkers. Thus, we believe LFSM-immunoassay is a highly promising method with broad applications for clinical testing.

Methods

Reagents and materials

Human cardiac troponin T (cTnT, catalog no. 8RTT5) was purchased from HyTest Ltd. Bovine serum albumin (BSA, catalog no. A7638-5G) and immunoglobulin G (IgG, catalog no. I2511-10MG) were purchased from Sigma-Aldrich. Human colostrum immunoglobulin A (IgA, catalog no. SIA1901-R22) and human plasma immunoglobulin M (IgM, catalog no. IP2020-03) were purchased from Athens Research and Technology. IL-6 monoclonal capture antibody (clone no. MQ2-13A5, catalog no. 14-7069) and detection antibody (clone no. MQ2-39C3, catalog no. 13-7068) were purchased from ThermoFisher Scientific. Recombinant human IL-6 protein (catalog no. 206-IL) was purchased from R&D Systems. PSA monoclonal capture antibody (clone no. M612165, catalog no. 10-P21A), detection antibody (clone no. M612166, catalog no. 10-P20A) and purified native human PSA protein (catalog no. 30-1205) were purchased from Fitzgerald Industries. Human NT-proBNP capture antibody (catalog no. BRJNBNPS108), detection antibody (catalog no. BRJNBNPS102) and recombinant protein (catalog no. GRCBNPS101) were purchased from Fapon International Limited. Reagent diluent (catalog no. DY995), streptavidin conjugated horseradish peroxidase (streptavidin-HRP, catalog no. DY998), stop solution (catalog no. DY994) and high-binding microplate (catalog no. DY990) were purchased from R&D systems. Gender unspecified pooled K2EDTA plasma from healthy human donors and gender unspecified pooled bovine whole blood were purchased from BioIVT Elevating Science. Heat-inactivated horse serum (catalog no. 26050) was purchased from ThermoFisher Scientific. ACS grade denatured ethanol (catalog no. BDH1158) was purchased from VWR International. N-hydroxysuccinimide (NHS, catalog no. 130672), N-(3-dimethylaminopropyl)-N-ethylcarbodiimide hydrochloride (EDC, catalog no. 03450), Amicon Ultra-0.5 mL centrifugal filters, 6-mercapto-1-hexanol (catalog no. 725226) and 8-mercaptooctanoic acid (catalog no. 675075) were purchased from Sigma-Aldrich (St. Louis, MO). Sylgard 184 Clear Silicone Elastomer Kit (catalog no. DC4019862) was purchased from Krayden Inc.

Microfluidic sensor chip fabrication

47 nm gold coated 24×50 mm^2 glass coverslip was used as the substrate of the sensor chip. The gold substrate was thoroughly rinsed with ethanol and deionized water sequentially and annealed using hydrogen flaming. The annealed gold substrate was then immersed overnight in an ethanol solution containing 100 μM 8-mercaptooctanoic acid (MOA) and 10 mM 6-mercapto-1-hexanol (MCH). After the gold substrate was thoroughly rinsed with ethanol and deionized water, a layer of 50 μm thick double-sided tape with a 3×36 mm^2 straight channel was adhered to the gold surface. Then, a 24×40 mm^2 glass coverslip with 2 drilled holes located at the 2 ends of the straight channel was placed onto the double-sided tape and pressed to form an enclosed microfluidic channel. To enable convenient fluid dispensing, 2 Polydimethylsiloxane (PDMS) pieces each with a punched through hole were bonded to the top surface of the glass coverslip with the through holes aligned. Finally, epoxy glue was applied to all the edges both of the top glass coverslip and the 2 PDMS pieces and cured for 1 hour at room temperature to secure and seal the sensor chip.

Sensor surface functionalization

The capture antibodies for IL-6, NT-proBNP and PSA were preprocessed by buffer exchange into MOPS buffer (5 mM MOPS, pH 7.4) with 5 spin cycles using Amicon centrifugal filters. 60 µL of an aqueous solution containing 5 mM EDC and 10 mM NHS was injected into the microfluidic channel and incubated for 5 min. Later, this procedure was repeated 2 more times to activate the carboxylic acid functional groups on the sensor surface. The channel was flushed with 200 µL MOPS buffer. In a 1-hour total incubation time, 100 µg/mL capture antibody in MOPS buffer was injected 3 times respectively at 0, 5 and 15 min with 20 µL volume used each time. Then, 100 µL aqueous solution containing 1 M ethanolamine with pH of 9.6 was injected to quench the unreacted NHS esters. Lastly, 500 µL of 1x phosphate buffered saline (PBS) was injected to flush the channel. The sensor chips were prepared prior to experiments and used within the same day.

Human IL-6 and PSA detection

For IL-6 detection in pure buffer, human recombinant IL-6 was spiked into 1x reagent diluent (1% BSA in 1x PBS) to reach final concentrations of 1, 10, 100, 10^3, 10^4, 10^5, 10^6, and 10^7 fM. For IL-6 detection in horse serum, 1, 10, 100, 10^3, and 10^4 fM of recombinant IL-6 were spiked into the horse serum. For IL-6 and PSA detection in bovine whole blood, the recombinant proteins of IL-6 or PSA were spiked so that the final concentrations for each whole blood samples were 1, 10, 100, 10^3, and 10^4 fM. The corresponding samples matrices without spiking were used as blank control to measure their background level. These spiked samples were injected through the sensor chips for 2 hours with a flow rate of 10 µL/min. Following a flushing step with 1x PBS, the chips were installed onto the PSM setup. 3 mL of 10 nM detection antibody in 1x PBS was flowed through the microfluidic channel for 10 min driven by gravity pump, while PSM images of the sensor surface was recorded in real time. The PSM images were then analyzed using an in-house dynamic tracking algorithm to count the number of detection antibodies binding to the sensor surface.

Human NT-proBNP detection and clinical evaluation

To generate the NT-proBNP calibration curve in human plasma, recombinant human NT-proBNP protein was spiked into the pooled human plasma to obtain spike-in concentrations of 1, 10, 100, 10^3, 10^4 and 10^5 pM. Baseline level of NT-proBNP in the pooled human plasma was 0.97 pM, determined by conventional ELISA. As such, the final concentrations of NT-proBNP in the spiked human plasma samples were 1.97, 10.97, 100.97, 10^3, 10^4 and 10^5 pM. These standard plasma samples were injected through the sensor chips for 10 min with a flow rate of 50 µL/min and then measured using PSM following the same procedure as in IL-6 detection. Under a protocol approved by the Mayo Clinic Institutional Review Board and Biospecimens Subcommittee (IRB # 19-002558/Bio00017399), 28 patient serum samples were deidentified and provided by Mayo Clinic Arizona. The patient samples were residual volume from routine clinical testing of NT-proBNP by Roche's Elecsys proBNP II assay. The samples were transported in icebox to our lab, stored at 4 °C and tested within 6 days using the LFSM-immunoassay.

Conventional ELISA measurement of NT-proBNP baseline

To measure the baseline NT-proBNP level in the spiking human plasma pool, a 96 well microplate was coated overnight with 100 µL of 2 µg/mL capture antibody of NT-proBNP in 1x PBS. After washed 3 times with 200 µL of 0.05% PBST (1x PBS containing 0.05% v/v Tween 20), the plate wells were blocked with 200 µL 1X reagent diluent for 1 hour. Then, a series of horse serum standard samples with spike-in NT-proBNP concentrations of 25, 50, 100, and 200 pg/mL were prepared. Horse serum without spiking was used as 0 pg/mL blank control. A mixture of 50 µL NT-proBNP-spiked horse serum standard sample or the human plasma and 50 µL biotinylated detection antibody (2 µg/mL) was incubated in the wells for 1 hour. Following another washing step as previously, 100 µL streptavidin-HRP solution was incubated in the wells for 20 min. Washed again with 0.05% PBST, the wells were reacted with 100 µL TMB substrate solution for 20 min. Lastly, 50 µL stop solution was added, followed by reading the absorbance of each well using a microplate reader (EnVision 2104, Perkin Elmer).

Experimental Setup

A 120 mW diode laser (L660P120, Thorlabs) with a central wavelength at 660 nm was used as the light source. The light was first collimated by a 20× objective and the beam size was reduced by a lens group. The sized-reduced beam was then focused on the prism surface by a short-focus lens with an incident angle of 71° to reach SPR. The scattered light from the biomolecule and gold surface was collected by a top-mounted 60× dry objective (Olympus, LUCPLFLN60X, NA = 0.7) equipped with a 180 mm tube lens to form an image on a CMOS camera (MQ013MG-ON, XIMEA). Additional details of the system layout can be found in Figure S1.

Image recording and processing

The raw image sequence was recorded by XIMEA CamTool at 60 frames per second, with an image size of 368 × 516 pixels. The images were processed by custom written Matlab scripts to extract the single protein binding events (See Figure S11 and S12 in the Supporting Information for details).

ASSOCIATED CONTENT

Supplementary Information

Supplementary Figures S1-S20, Supplementary Tables 1 – 2, Supplementary Notes 1 – 6 and Supplementary Movies of specific and non-specific binding events.

Author Contributions

S.W. and X.Z. conceived the project. X.Z., G.M. and S.W. built the instrument, X.Z., C.C. and S.W. designed the experiments, X.Z. and C.C. carried out the experiments, X.Z., and S.W. analyzed the data, C.C., M.J., B.B. and Z.W. fabricated the gold coated sensor chips, C.S. and E.Y.

provided the clinical samples and corresponding validation data, S.W. supervised the project, X.Z., C.C. and S.W. wrote the paper, all authors reviewed the paper.

Notes

The authors declare the following competing financial interest(s): S. W. is a member of the technology advisory board of Biosensing Instrument Inc.

Acknowledgement

We acknowledge financial support from faculty startup package for S.W., the National Institute of General Medical Sciences of the National Institutes of Health Award R01GM140193, and Mayo Clinic Arizona Cardiovascular Clinical Research Center Grant ARI-285360-01. We also acknowledge the use of facilities within the ASU NanoFab supported in part by NSF program NNCI-ECCS-1542160.

References

1 Mordente, A., Meucci, E., Martorana, G. E. & Silvestrini, A. Cancer biomarkers discovery and validation: state of the art, problems and future perspectives. *Advances in Cancer Biomarkers: From biochemistry to clinic for a critical revision*, 9-26 (2015).

2 Kim, S.-H., Hoffmann, U., Borggrefe, M., Akin, I. & Behnes, M. Advantages and limitations of current biomarker research: from experimental research to clinical application. *Current pharmaceutical biotechnology* **18**, 445-455 (2017).

3 Solier, C. & Langen, H. Antibody-based proteomics and biomarker research—current status and limitations. *Proteomics* **14**, 774-783 (2014).

4 Belanger, L., Sylvestre, C. & Dufour, D. Enzyme-linked immunoassay for alpha-fetoprotein by competitive and sandwich procedures. *Clinica chimica acta* **48**, 15-18 (1973).

5 Farajollahi, M. M., Cook, D. B., Hamzehlou, S. & Self, C. H. Reduction of non-specific binding in immunoassays requiring long incubations. *Scandinavian journal of clinical and laboratory investigation* **72**, 531-539 (2012).

6 Giljohann, D. A. & Mirkin, C. A. Drivers of biodiagnostic development. *Nature* **462**, 461-464 (2009).

7 Shashkova, S. & Leake, M. C. Single-molecule fluorescence microscopy review: shedding new light on old problems. *Bioscience reports* **37**, BSR20170031 (2017).

8 Rissin, D. M. *et al.* Single-molecule enzyme-linked immunosorbent assay detects serum proteins at subfemtomolar concentrations. *Nature Biotechnology* **28**, 595-599 (2010). https://doi.org:10.1038/nbt.1641

9 Johnson-Buck, A. *et al.* Kinetic fingerprinting to identify and count single nucleic acids. *Nature Biotechnology* **33**, 730-732 (2015). https://doi.org:10.1038/nbt.3246

10 Mao, C.-P. *et al.* Protein detection in blood with single-molecule imaging. *Science Advances* **7**, eabg6522 https://doi.org:10.1126/sciadv.abg6522

11 Jing, W. *et al.* Time-resolved digital immunoassay for rapid and sensitive quantitation of procalcitonin with plasmonic imaging. *ACS nano* **13**, 8609-8617 (2019).

12 Zhang, P. *et al.* Plasmonic scattering imaging of single proteins and binding kinetics. *Nature Methods* **17**, 1010-1017 (2020). https://doi.org:10.1038/s41592-020-0947-0

13 Zhang, P., Ma, G., Wan, Z. & Wang, S. Quantification of Single-Molecule Protein Binding Kinetics in Complex Media with Prism-Coupled Plasmonic Scattering Imaging. *ACS Sensors* **6**, 1357-1366 (2021). https://doi.org:10.1021/acssensors.0c02729

14 Yang, L. *et al.* An adaptive non-local means filter for denoising live-cell images and improving particle detection. *Journal of Structural Biology* **172**, 233-243 (2010). https://doi.org:https://doi.org/10.1016/j.jsb.2010.06.019
15 Cole, D., Young, G., Weigel, A., Sebesta, A. & Kukura, P. Label-Free Single-Molecule Imaging with Numerical-Aperture-Shaped Interferometric Scattering Microscopy. *ACS Photonics* **4**, 211-216 (2017). https://doi.org:10.1021/acsphotonics.6b00912
16 Young, G. *et al.* Quantitative mass imaging of single biological macromolecules. *Science* **360**, 423-427 (2018). https://doi.org:10.1126/science.aar5839
17 Ma, G., Zhang, P., Zhou, X., Wan, Z. & Wang, S. Label-Free Single-Molecule Pulldown for the Detection of Released Cellular Protein Complexes. *ACS Central Science* **8**, 1272-1281 (2022). https://doi.org:10.1021/acscentsci.2c00602
18 Tanaka, T., Narazaki, M. & Kishimoto, T. IL-6 in inflammation, immunity, and disease. *Cold Spring Harbor perspectives in biology* **6**, a016295 (2014).
19 Narazaki, M., Tanaka, T. & Kishimoto, T. The role and therapeutic targeting of IL-6 in rheumatoid arthritis. *Expert review of clinical immunology* **13**, 535-551 (2017).
20 Coomes, E. A. & Haghbayan, H. Interleukin-6 in COVID-19: a systematic review and meta-analysis. *Reviews in medical virology* **30**, 1-9 (2020).
21 Nair, R. *et al.* Reducing All-cause 30-day Hospital Readmissions for Patients Presenting with Acute Heart Failure Exacerbations: A Quality Improvement Initiative. *Cureus* **12**, e7420 (2020). https://doi.org:10.7759/cureus.7420
22 Ziaeian, B. & Fonarow, G. C. The Prevention of Hospital Readmissions in Heart Failure. *Progress in Cardiovascular Diseases* **58**, 379-385 (2016). https://doi.org:https://doi.org/10.1016/j.pcad.2015.09.004
23 Ponikowski, P. *et al.* 2016 ESC Guidelines for the diagnosis and treatment of acute and chronic heart failure: The Task Force for the diagnosis and treatment of acute and chronic heart failure of the European Society of Cardiology (ESC)Developed with the special contribution of the Heart Failure Association (HFA) of the ESC. *European Heart Journal* **37**, 2129-2200 (2016). https://doi.org:10.1093/eurheartj/ehw128
24 Hall, C. Essential biochemistry and physiology of (NT-pro)BNP. *European Journal of Heart Failure* **6**, 257-260 (2004). https://doi.org:https://doi.org/10.1016/j.ejheart.2003.12.015
25 McKie, P. M. & Burnett, J. C. NT-proBNP: The Gold Standard Biomarker in Heart Failure∗. *Journal of the American College of Cardiology* **68**, 2437-2439 (2016). https://doi.org:https://doi.org/10.1016/j.jacc.2016.10.001
26 Vashist, S. K., Luppa, P. B., Yeo, L. Y., Ozcan, A. & Luong, J. H. T. Emerging Technologies for Next-Generation Point-of-Care Testing. *Trends in Biotechnology* **33**, 692-705 (2015). https://doi.org:https://doi.org/10.1016/j.tibtech.2015.09.001
27 Li, S. *et al.* Electrochemical Biosensors for Whole Blood Analysis: Recent Progress, Challenges, and Future Perspectives. *Chemical Reviews* **123**, 7953-8039 (2023). https://doi.org:10.1021/acs.chemrev.1c00759
28 Litwin, M. S. & Tan, H.-J. The diagnosis and treatment of prostate cancer: a review. *Jama* **317**, 2532-2542 (2017).
29 Schröder, F. H. *et al.* Screening and prostate cancer mortality: results of the European Randomised Study of Screening for Prostate Cancer (ERSPC) at 13 years of follow-up. *The Lancet* **384**, 2027-2035 (2014).
30 Schröder, F. H. *et al.* Screening and prostate-cancer mortality in a randomized European study. *New England journal of medicine* **360**, 1320-1328 (2009).
31 Lilja, H., Ulmert, D. & Vickers, A. J. Prostate-specific antigen and prostate cancer: prediction, detection and monitoring. *Nature Reviews Cancer* **8**, 268-278 (2008).
32 Zeng, Q. *et al.* Dynamic single-molecule sensing by actively tuning binding kinetics for ultrasensitive biomarker detection. *Proceedings of the National Academy of Sciences* **119**, e2120379119 (2022). https://doi.org:10.1073/pnas.2120379119

33 Wang, R. *et al.* Rapid Regulation of Local Temperature and Transient Receptor Potential Vanilloid 1 Ion Channels with Wide-Field Plasmonic Thermal Microscopy. *Analytical Chemistry* **94**, 14503-14508 (2022). https://doi.org:10.1021/acs.analchem.2c03111
34 Dahmardeh, M., Mirzaalian Dastjerdi, H., Mazal, H., Köstler, H. & Sandoghdar, V. Self-supervised machine learning pushes the sensitivity limit in label-free detection of single proteins below 10 kDa. *Nature Methods* **20**, 442-447 (2023). https://doi.org:10.1038/s41592-023-01778-2
35 Zhang, P. *et al.* Evanescent scattering imaging of single protein binding kinetics and DNA conformation changes. *Nat Commun* **13**, 2298 (2022). https://doi.org:10.1038/s41467-022-30046-8
36 Landry, J. P., Ke, Y., Yu, G. L. & Zhu, X. D. Measuring affinity constants of 1450 monoclonal antibodies to peptide targets with a microarray-based label-free assay platform. *J Immunol Methods* **417**, 86-96 (2015). https://doi.org:10.1016/j.jim.2014.12.011
37 Yang, X. *et al.* High-affinity binding to the SARS-CoV-2 spike trimer by a nanostructured, trivalent protein-DNA synthetic antibody. *bioRxiv*, 2023.2009.2018.558353 (2023). https://doi.org:10.1101/2023.09.18.558353
38 Cole, D., Young, G., Hundt, N. & Kukura, P. Interferometric Scattering Mass Spectrometry (ISCAMS): Single Molecule Mass Imaging in Solution. *Biophysical Journal* **114**, 682a (2018).
39 Singh, P. SPR biosensors: historical perspectives and current challenges. *Sensors and actuators B: Chemical* **229**, 110-130 (2016).
40 Zhou, J. *et al.* Surface plasmon resonance (SPR) biosensors for food allergen detection in food matrices. *Biosensors and Bioelectronics* **142**, 111449 (2019).

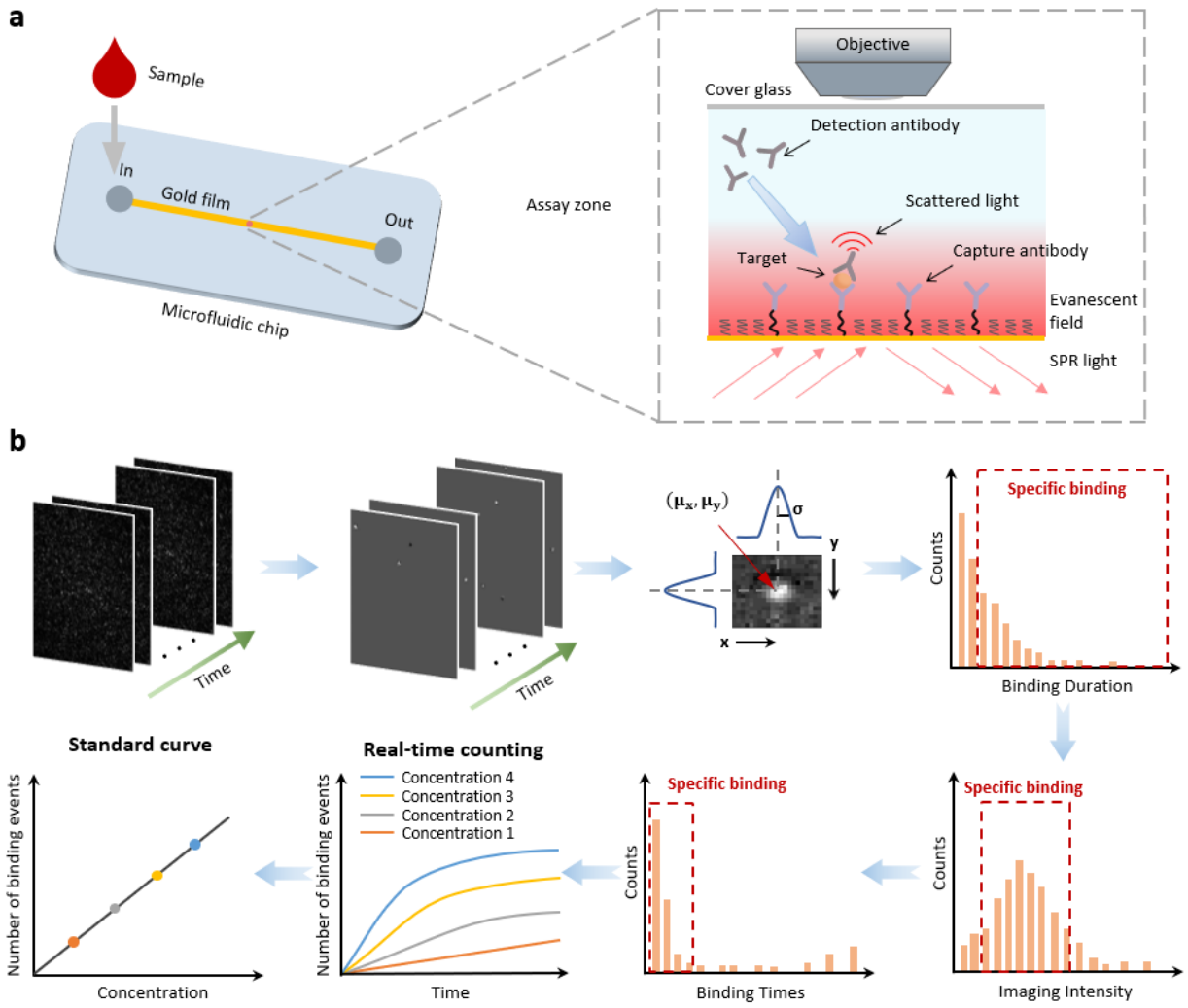

Figure 1. The principle of LFSM-immunoassay. (a) Experimental setup. The analytes of interest are first pulled down by the capture antibodies tethered to the gold film via an alkane linker. A P-polarized incident light is focused on the gold surface with an incident angle of 71° to excite SPR and the associated evanescent field. After introducing detection antibody solution, the process of detection antibody binding to the biomarkers caught on the surface is recorded by a CMOS camera via an air objective above the microfluidic channel. (b) The raw images are processed by a custom-written algorithm to remove background noise and extract the binding events of single particles hitting the sensor surface. A time course of the total count of the specific binding of detection antibody is then determined after filtering in terms of the position, molecular weight, binding duration, and binding frequency of the detected binding events is applied. Finally, a standard curve (binding events vs analyte concentration) is generated from triplicate tests for different analyte concentrations. More details are provided in Supplementary Note 2.

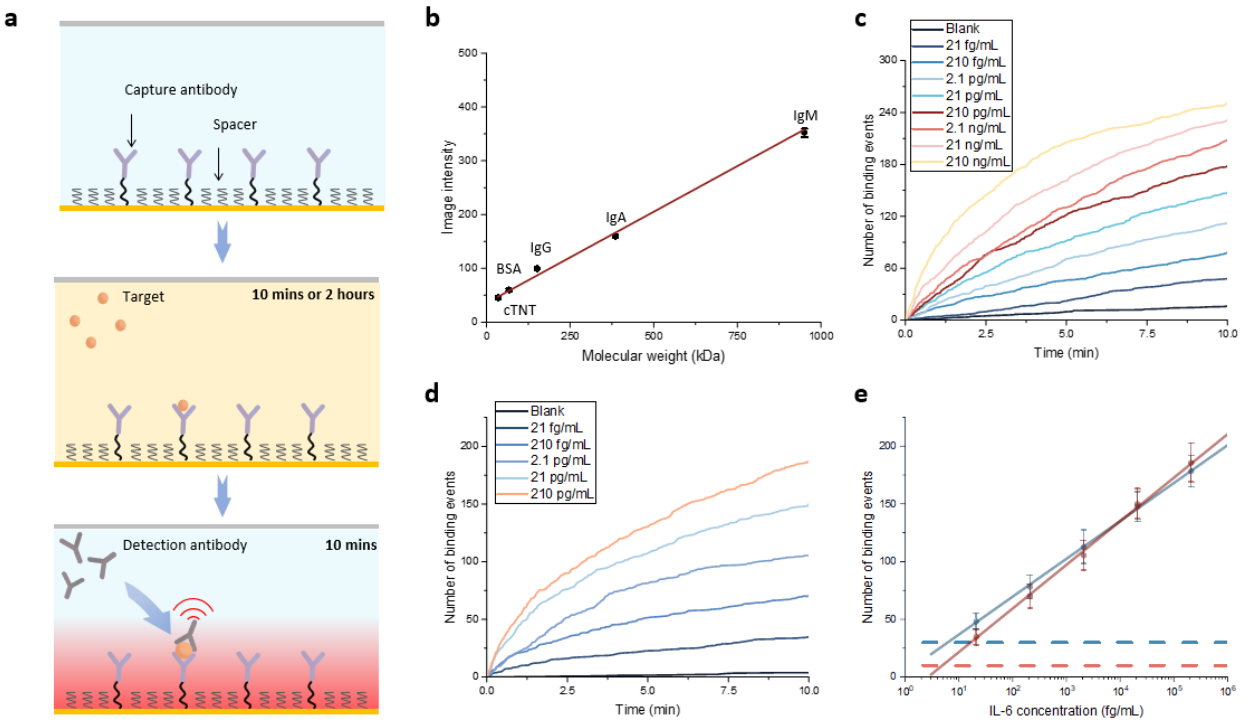

Figure 2. Validation of LFSM-immunoassay. (a) Workflow of LFSM-immunoassay. Capture antibodies were first immobilized on the gold film through alkane linker. Analyte samples were flowed through the microfluidic channel for 10 minutes in NT-proBNP detection or 2 hours in the other cases. 10 nM detection antibody solution was injected for 10 minutes and the binding of detection antibody to analytes captured on the sensor surface was recorded. (b) The relationship between PSM image intensity and the molecular weight (MW) of particles, determined from PSM images of different proteins in PBS solution. The mean intensity of one type of protein is the mean of its Gaussian fit to the corresponding histograms in Figure S2. The error bars are the model fitting error in Figure S2. The number of total binding events over time for different IL-6 concentrations in (c) pure buffer and (d) bovine serum. For clarity, the means of triplicate tests were plotted. (e) Standard curves of IL-6 detection in pure buffer (blue) and bovine serum (red). The error bars are the standard deviation of triplicate experiments. The blue and red dashed line represent the limit of detection for pure buffer and bovine serum respectively, defined as mean + 3×s.d. counts of blank solution.

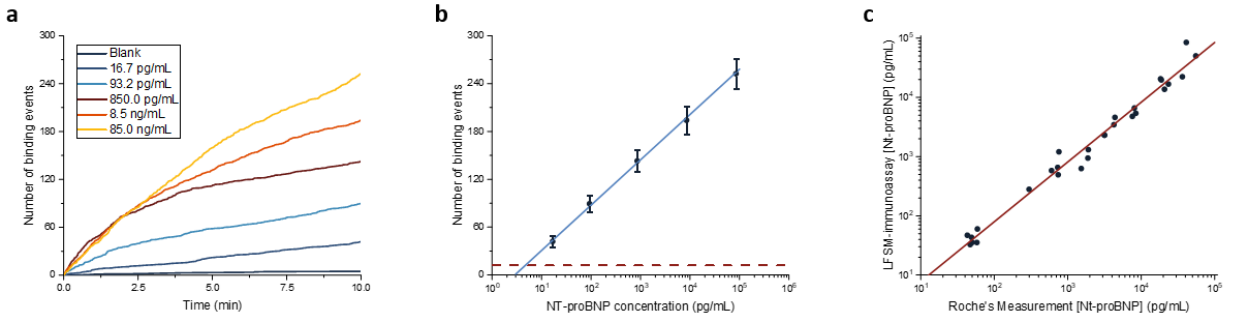

d

Patient ID	[NT-proBNP] (pg/mL)	Roche's result (pg/mL)	Patient ID	[NT-proBNP] (pg/mL)	Roche's result (pg/mL)	Patient ID	[NT-proBNP] (pg/mL)	Roche's result (pg/mL)	Patient ID	[NT-proBNP] (pg/mL)	Roche's result (pg/mL)
1	32.64	47	8	2302.90	3161	15	3454.25	4253	22	628.72	1527
2	13709.94	20792	9	35.37	58	16	22301.67	36348	23	492.98	741
3	4777.73	7586	10	1305.45	1910	17	84855.03	41105	24	59.89	59
4	655.25	731	11	279.70	298	18	16767.70	23497	25	20564.14	18356
5	6608.29	8090	12	43.29	49	19	19719.41	18795	26	4587.88	4389
6	50176.41	55506	13	35.37	50	20	5389.28	8456	27	1203.75	759
7	580.22	603	14	943.89	1880	21	2300.51	3178	28	46.97	43

Figure 3. Rapid NT-proBNP detection in human plasma and clinical evaluation. (a) Temporal profiles for different NT-proBNP concentrations in human plasma. For clarity, the mean of triplicate tests were plotted. (b) Standard curve of NT-proBNP detection in human plasma. The error bars were s.d. of 3 replicates. The dashed line represents the limit of detection for NT-proBNP in human plasma, defined as mean + 3×s.d. counts of blank solution (horse serum). (c) Pearson's correlation between LFSM-immunoassay and Roche's Elecsys proBNP II assay. The results were determined from measurements of serum samples from 28 patients using both the Elecsys proBNP II assay and LFSM-immunoassay. (d) Summary of all the LFSM-immunoassay measurement results and corresponding Roche assay results for the 28 patients.

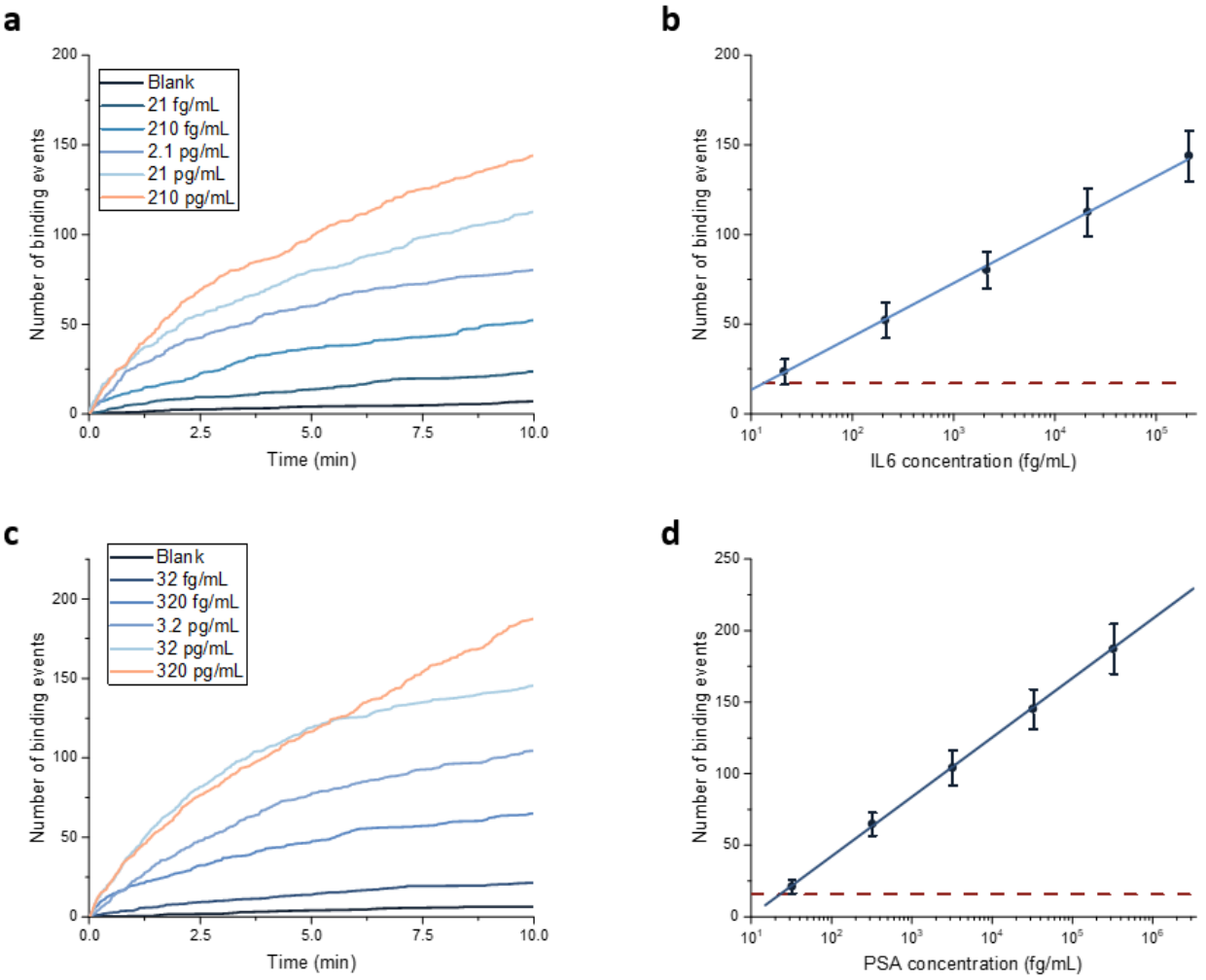

Figure 4. Protein biomarkers detection in whole blood. Time courses of total binding events for different concentrations of (a) IL-6 and (c) PSA in bovine whole blood. For clarity, the mean count of triplicate tests were plotted. Standard curve of (b) IL-6 and (d) PSA in bovine whole blood. Error bars are s.d. of three replicates. The red dashed line represents the limit of detection, defined as mean + 3×s.d. counts of blank solution.